Selective Dimerization of Ethene to 2-Butene on Zn^{2+}-Modified ZSM-5 Zeolite

Lashchinskaya, Zoya N.; Gabrienko, Anton A.; Kolganov, Alexander A.; Pidko, Evgeny A.; Stepanov, Alexander G.

DOI
10.1021/acs.jpcc.2c01101

Publication date
2022

Document Version
Final published version

Published in
Journal of Physical Chemistry C

THE JOURNAL OF PHYSICAL CHEMISTRY C
A JOURNAL OF THE AMERICAN CHEMICAL SOCIETY

pubs.acs.org/JPCC

Article

Selective Dimerization of Ethene to 2-Butene on Zn^{2+}-Modified ZSM-5 Zeolite

Zoya N. Lashchinskaya, Anton A. Gabrienko,* Alexander A. Kolganov, Evgeny A. Pidko, and Alexander G. Stepanov*

Cite This: *J. Phys. Chem. C* 2022, 126, 6570−6577

Read Online

ACCESS | Metrics & More | Article Recommendations | Supporting Information

ABSTRACT: Selective dimerization of ethene to 2-butene on Zn^{2+}-containing ZSM-5 zeolite (Zn^{2+}/ZSM-5) at 296−523 K has been discovered. The intermediate but-3-en-1-ylzinc species is identified with ^{13}C CP/MAS NMR and Fourier transform infrared spectroscopy. The density functional theory study of two alternative dimerization pathways reveals that the intermediate is formed with the involvement of the saturated bridged dimeric Zn−$(CH_2)_4$−O species. It is also shown that ethene conversion to 2-butene increases with the increase in the quantity of Brønsted acid sites in Zn^{2+}/ZSM-5 zeolite; however, the selectivity of the reaction decreases. The results obtained are of potential interest for developing industrially relevant Zn-containing zeolite catalysts for the selective conversion of ethene to 2-butene.

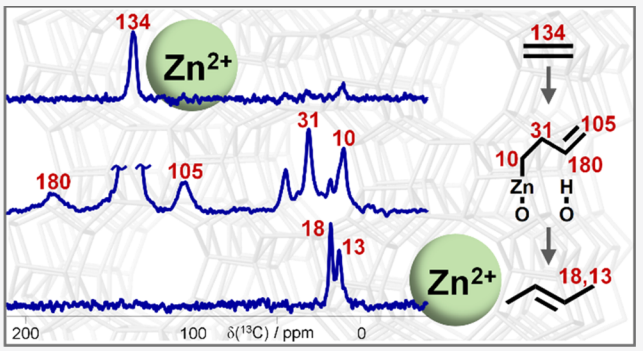

1. INTRODUCTION

The modern chemical industry requires the synthesis of significant amounts of linear butenes to be widely used in manufacturing polymers and other valuable chemicals (plasticizers, antioxidants, oils, etc.).[1] One of the options for the synthesis of 1- and 2-butene is the dimerization of ethene,[1−3] which is an abundant raw material. Several catalysts based on different transition metals (Co, Ni, Pd, Rh, and Zr) with or without alkylaluminum co-catalysts have been tested for ethene dimerization.[1,4] Among the catalysts used, Ni-based systems dominate this field both in homogeneous and heterogeneous catalysis.[2−4] Because nickel complexes are often stable only at low temperatures, heterogeneous catalysts such as nickel supported on silica, silica-alumina, zeolites, and mesoporous materials are preferred.[5−11] Despite the notable development in Ni-modified zeolite synthesis and investigation, some limitations exist concerning the selectivity toward the target product and the catalyst stability. Furthermore, the nature of the active species and the mechanism of dimerization are still under discussion.[8,11,12] Moreover, Ni-containing catalysts provide quite selective 1-butene formation, whereas 2-butene is also in demand for the polymer industry. In this regard, it is of particular interest to search for alternative catalytic systems capable of converting ethene to 2-butene.

Zn-containing zeolites provide the strong interaction of Zn^{2+} cations with C_3−C_4 alkenes, giving very stable π-complexes.[13−15] This interaction facilitates di- and trimerization of the alkenes with the involvement of Zn^{2+} cations and prevents alkene oligomerization on Brønsted acid sites (BAS). Therefore, it is appealing to test a Zn-modified zeolite for ethene dimerization.

In this work, Zn^{2+}-modified ZSM-5 zeolite is investigated with respect to ethene transformation. We demonstrate for the first time the potential of Zn-loaded zeolites to perform remarkably selective ethene dimerization to 2-butene. To gain insights into the reaction mechanism, a combination of experimental and computational techniques was applied. Solid-state NMR spectroscopy (^1H and ^{13}C MAS NMR) was used to follow the pathway of ethene transformation with the assistance of Zn^{2+} sites and detect the reaction intermediate. To further clarify the structure of the intermediate, Fourier transform infrared (FTIR) spectroscopy was used. The alternative pathways of the detected intermediate formation were examined with density functional theory (DFT) calculations.

2. EXPERIMENTAL SECTION

2.1. Materials and Reagents. Ethene−$^{13}C_1$ (99% ^{13}C isotope enrichment), benzene−$^{13}C_6$ (99% ^{13}C isotope enrichment), ethene, and metallic zinc were purchased from Aldrich Chemical Co. Inc. and were used without further purification.

Received: February 15, 2022
Revised: March 25, 2022
Published: April 6, 2022

https://doi.org/10.1021/acs.jpcc.2c01101
J. Phys. Chem. C 2022, 126, 6570−6577

Industrially produced *n*-butene (thermodynamic mixture, trans/cis/1-butene = 100:26:4)[16] was used after purification from possible traces of water vapor or other impurities via freezing and thawing in the liquid nitrogen trap.

2.2. Zeolite Sample Preparation. The parent H-ZSM-5 zeolite, Si/Al = 12, was kindly provided by Tricat Zeolites. Before use, the zeolite powder was calcined in airflow at 773 K. The zeolite sample was characterized in detail, with the results being presented in our earlier works (see, e.g., ref 13). The Si/Al ratio was determined with ^{29}Si MAS NMR, while the content of extra-framework aluminum was obtained with ^{27}Al MAS NMR.[15] The concentration of BAS in the parent H-ZSM-5 was measured with the ^{1}H MAS NMR approach using methane and benzene as internal standards.[17,18] The composition of the unit cell was calculated on the basis of the Si/Al ratio. Table 1 demonstrates the main characteristics of the parent and Zn-modified ZSM-5 zeolite samples.

Table 1. Properties of the Parent and Zn-Modified Zeolite Samples

zeolite sample	Si/Al	Zn/wt %[a]	Si−O(H)−Al/μmol g^{-1}	zeolite unit cell
H-ZSM-5	12		1290	$Al_{0.5}^{oct}$ $H_{7.4}$ $Al_{7.4}$ $Si_{88.6}$ O_{192}
Zn^{2+}/ZSM-5	12	3.6	150	$Zn_{3.3}$ $Al_{0.5}^{oct}$ $H_{0.9}$ $Al_{7.4}$ $Si_{88.6}$ O_{192}
Zn^{2+}/H-ZSM-5	12	0.9	1010	$Zn_{0.8}$ $Al_{0.5}^{oct}$ $H_{5.9}$ $Al_{7.4}$ $Si_{88.6}$ O_{192}

[a]Calculated from the unit cell composition.

To introduce isolated Zn^{2+} cations, the method of H-ZSM-5 reaction with Zn vapor was applied.[19−22] Before the reaction, the parent zeolite was activated via evacuation at 673 K for 16 h (residual pressure < 10^{-2} Pa). After the activation, the reaction between H-ZSM-5 and zinc vapor was carried out in a vacuumed glassware at 773 K for 2 h followed by evacuation at 773 K for 20 h to remove molecular hydrogen and unreacted zinc. To study the particular effects of Zn sites and BAS on ethene transformation, two samples of Zn-modified ZSM-5 zeolite were prepared with different degrees of BAS exchange for Zn^{2+} cations. To synthesize ZSM-5 zeolite with the minimum BAS content, the excess of metallic zinc (the ratio Zn/Al = 2.8) was used. This sample was designated as Zn^{2+}/ZSM-5. To obtain a zeolite sample with appreciable amounts of both BAS and Zn^{2+} sites, the ratio Zn/Al was chosen to be 0.13. This sample was designated as Zn^{2+}/H-ZSM-5.

The concentration of residual BAS [Si−O(H)−Al groups] in both samples was determined with the ^{1}H MAS NMR approach[17,18] using benzene−$^{13}C_6$ as an internal standard. The known amount of benzene-$^{13}C_6$ was loaded into the ampoules with Zn^{2+}-modified ZSM-5 samples (the pressure was controlled with vacuum gauge, Thermovac 101, Leybold, Germany). Afterward, the ampoules were sealed with a torch flame and heated at 373 K for 46 h to achieve benzene uniform distribution over the zeolite pore volume. ^{1}H MAS NMR spectra of the zeolite samples with adsorbed benzene−$^{13}C_6$ are presented in Figure S1. It was obtained that the concentration of BAS amounted to 150 μmol g^{-1} in Zn^{2+}/ZSM-5 and 1010 μmol g^{-1} in Zn^{2+}/H-ZSM-5 (Table 1), giving the degree of BAS exchange for zinc cations 88 and 22%, respectively. It was decided to use ^{13}C-labeled benzene to record high-quality ^{13}C CP/MAS NMR spectra of the samples and ensure that benzene did not react under these conditions and represented an appropriate internal standard for OH concentration measurements. Indeed, the related spectra (not shown) contain only the signal from benzene at 132 ppm. The unit cell of Zn-modified samples was calculated taking into account both the residual BAS concentration and the quantity of the loaded Zn (Table 1).

2.3. Sample Preparation for MAS NMR Experiments. To prepare the samples for MAS NMR measurements, the powder of the activated zeolite sample, Zn^{2+}/ZSM-5 or Zn^{2+}/H-ZSM-5, was placed into a highly symmetrical ampoule, 3.5 mm in diameter, made of Pyrex glass. Such ampoules fit tightly into a 4 mm MAS NMR rotor and can be spun at high speed to obtain high-resolution solid-state NMR spectra. The adsorption of ethene−$^{13}C_1$ was performed as follows. First, the required amount of the reagent was loaded to the calibrated volume (the pressure was controlled with a vacuum gauge, Thermovac 101, Leybold, Germany). Second, ethene was transferred to the zeolite sample by the ampule freezing with liquid N_2. Eventually, the ampule with ethene adsorbed on the Zn-containing zeolite sample was sealed with a torch flame and kept in liquid N_2 to prevent any transformation of the alkene. The total concentration of ethene amounted to 316 μmol per gram of the Zn-modified zeolite.

2.4. MAS NMR Measurements. MAS NMR spectra were recorded at 296 K on a Bruker Avance-400 spectrometer (9.4 T), equipped with a broad band double-resonance 4 mm MAS NMR probe. ^{1}H MAS NMR spectra (the resonance frequency of 400.13 MHz) were recorded with a 60 s delay between the scans and a spinning rate of 7 kHz, and 16 scans were accumulated for one spectrum. To obtain ^{13}C (CP) MAS NMR spectra at the resonance frequency of 100.63 MHz, the NMR rotors with the glass ampoules were spun at 9 kHz with dry compressed air. To suppress spin−spin coupling, high-power proton decoupling was applied at the power level corresponding to 5.0 μs length of 90° ^{1}H pulse and nutation frequency of 50 kHz. For each ^{13}C MAS NMR spectrum, 2000 scans were acquired (5 s repetition delay) with a 5.4 μs 90° excitation pulse. ^{13}C CP/MAS NMR spectra (20000−70000 scans with a 2 s delay) were recorded with the contact time of 2 ms at the Hartmann−Hahn matching condition of 50 kHz. Tetramethylsilane was used as an external standard to determine ^{1}H and ^{13}C chemical shifts with an accuracy of ±0.1 ppm. The parameters of ^{13}C CP/MAS NMR were optimized using adamantane as the standard.

2.5. FTIR Spectroscopy. Ethene transformation on a Zn^{2+}/ZSM-5 sample was additionally investigated with FTIR spectroscopy. First, the parent H-ZSM-5 zeolite was pressed in a self-supporting wafer, 12.3 mg cm^{-2} in density, and placed to the homemade quartz holder. The zeolite sample was activated via gradual heating to 673 K (1 K min^{-1}) under vacuum and further evacuation at 673 K for 16 h (residual pressure < 10^{-2} Pa). To introduce isolated Zn^{2+} cations, the excess of metallic zinc (Zn/Al = 22) was transferred to the zeolite wafer in a sealed glass system and heated at 773 K for 1 h followed by evacuation at 773 K for 5 h. Afterward, the wafer in the holder was transferred into the homemade IR cell (CaF_2 windows) in a glove box under Ar. To remove Ar and possible water impurities, the sample was later evacuated at 723 K for 2.5 h. The IR cell was connected to a valve for gaseous reagent dosage and a special compartment for ex situ sample heating.

https://doi.org/10.1021/acs.jpcc.2c01101
J. Phys. Chem. C 2022, 126, 6570−6577

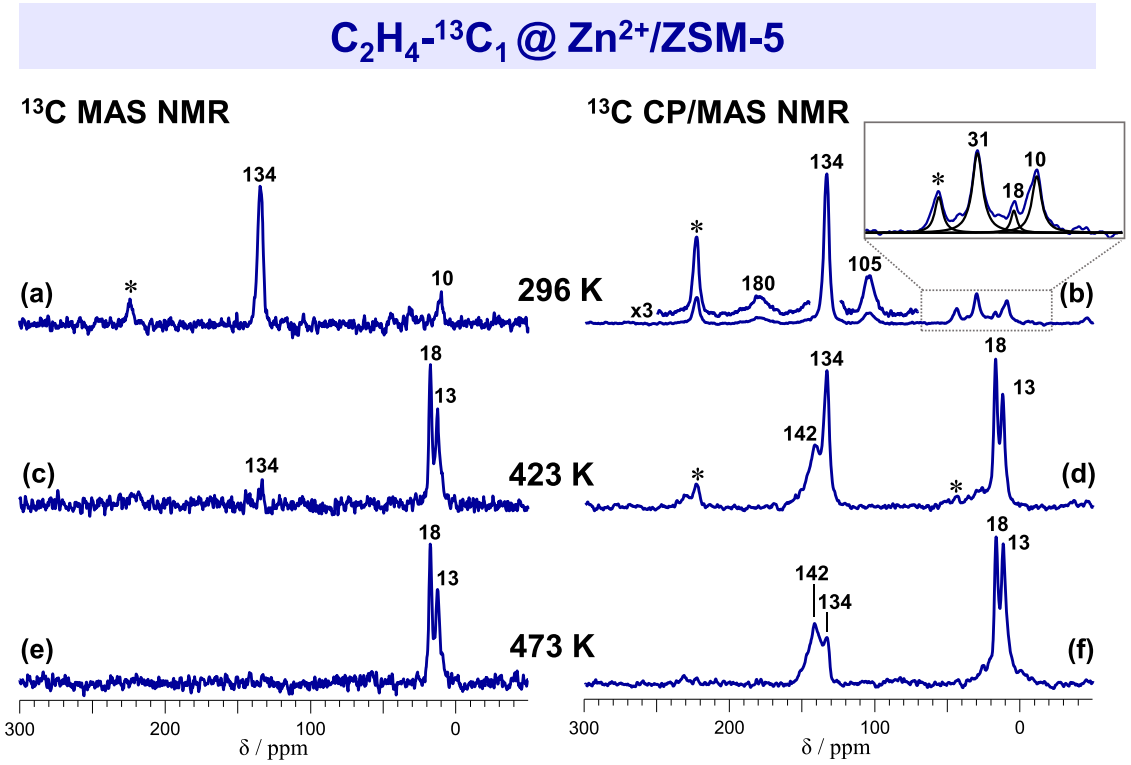

Figure 1. ^{13}C MAS NMR (a,c,e) and ^{13}C CP/MAS NMR (b,d,f) spectra of ethene−$^{13}C_1$ adsorbed on Zn^{2+}/ZSM-5 zeolite. The sample was successively heated ex situ for 5 min at 296 (a,b), 423 (c,d), and 473 K (e,f). Asterisks (*) denote spinning sidebands.

FTIR spectra were recorded on a Shimadzu IRTracer-100 FTIR spectrophotometer equipped with a purge control kit PCK-100. Purging of the sample compartment, detector, and interferometer with Ar flow was carried out before and during the spectra acquisition to minimize the effect of atmospheric water and CO_2 on the resulting FTIR spectra. The spectral range was chosen to be 1100−4000 cm^{-1}, with the resolution being 4 cm^{-1}. For each spectrum, 500 scans were accumulated. The spectrum of the pure Zn^{2+}/ZSM-5 zeolite was first recorded. Then, incremental amounts of ethene were adsorbed from the gas phase on the zeolite wafer held in liquid N_2 to achieve the total ethene concentration of 50, 100, 300, and 500 μmol g^{-1}, with the FTIR spectrum being acquired after each dosage. To monitor ethene transformation at 373−623 K, the wafer was transferred to the special compartment, heated at the required temperature, cooled to 296 K, and transferred back to the IR cell followed by spectrum recording. The same procedure was applied to perform the experiments with *n*-butene.

2.6. DFT Calculations. *2.6.1. Computational Model.* The molecular cluster containing 66 T-atoms (Figure S2a) was constructed from the MFI framework structure obtained from the Database of Zeolite Structures.[23] Dangling O-atoms were substituted by H atoms at 1.47 Å distance from a neighboring Si-atom.[24] To compensate for the charge of the Zn^{2+} cation, two aluminum atoms were placed at the T7 and T12 positions (Figure S2b).[25]

2.6.2. Computational Methods. DFT spin-unrestricted calculations were carried out using the ORCA 5.0.1 program package.[26,27] PBE0 hybrid exchange-correlational functional[28] with D3BJ dispersion correction[29,30] was used to describe the exchange-correlational term. The 6-31G* basis set[31−33] was used for the framework atoms (Si, Al, O, and $H_{terminal}$), while the def2-TZVP[34,35] one was used for the atoms of the extra-framework species (Zn, C, and H). The geometry of the models was considered optimized when the RMS energy gradient and maximum energy gradient were less than 5×10^{-6} and 5×10^{-5} a.u., respectively. During the geometry optimization, the cartesian coordinates of the terminal H-atoms were fixed.

Transition states were identified using the CI-NEB procedure as implemented in ORCA.[36] The structure of these states was confirmed by the presence of only one imaginary frequency along the reaction coordinate in the vibrational spectra. These spectra were calculated using the partial hessian vibrational analysis (PHVA). During PHVA, only extra-framework atoms were allowed to relax.

Note that the discussion on the reaction mechanisms has been based on the relative electronic energies, which provide the same qualitative picture for the reaction profile as the free energies, because the entropy effect is usually minor.[37,38]

3. RESULTS AND DISCUSSION

Figure 1 shows ^{13}C (CP) MAS NMR spectra of ethene−$^{13}C_1$ adsorbed on the Zn^{2+}/ZSM-5 zeolite with high content of Zn^{2+} cations (Table 1, Figure S1). At 296 K, mainly, the signal at 134 ppm of the adsorbed ethene is detected in the spectra (Figure 1a,b). The significant downfield shift of the ethene signal with respect to that expected in solution (123.5 ppm)[39] is accounted for by the C=C bond perturbation due to the formation of the π-complex with Zn^{2+} cations.[40] The ^{13}C CP/MAS NMR spectrum (Figure 1b), which emphasizes strongly adsorbed and immobile species, contains additional minor signals at 10, 18, 31, 105, and 180 ppm. The comparison of the ^{1}H MAS NMR spectrum of ethene on Zn^{2+}/ZSM-5 with that of pure zeolite (Figure S3) reveals that some additional

https://doi.org/10.1021/acs.jpcc.2c01101
J. Phys. Chem. C 2022, 126, 6570−6577

Scheme 1. Alternative Structures of the Ethene Dimerization Intermediate Detected with ^{13}C MAS NMR; Assigned ^{13}C Chemical Shifts Are Shown in Red

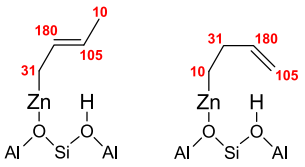

amount of BAS is formed at ethene adsorption. At 423−473 K (Figure 1c−f), the signals of 2-butene are detected in the spectra, with no other products formed from ethene being observed. The signal at 142 ppm belongs to C=C atoms, while those at 18 and 13 ppm arise from the methyl groups of *trans*- and *cis*-2-butene, respectively.[14,41] This is unequivocal evidence for the selective ethene dimerization to 2-butene on Zn^{2+}/ZSM-5 at $T \leq 473$ K.

The formation of 2-butene was observed on Zn^{2+}/H-ZSM-5 zeolite with the larger quantity of BAS (Table 1, Figure S1) at 296 K (Figure S4). However, no specific signals at 10, 31, 105, and 180 ppm were detected. Also, further transformation of 2-butene occurs on Zn^{2+}/H-ZSM-5 at $T \geq 423$ K as seen by the signals at 26−30, 93, and 115 ppm[14] (Figure S4). Therefore, the larger quantity of BAS increases ethene conversion to 2-butene but decreases the dimerization selectivity at the expense of the oligomerization process at $T \geq 423$ K.

The four signals at 10, 31, 105, and 180 ppm, disappearing at $T > 296$ K, should belong to some intermediate preceding the formation of 2-butene (Figure 1b). Because the generation of additional BAS upon ethene adsorption was detected (vide supra), the formation of the Zn-attached C_4-intermediate can be assumed. Additionally, the observed chemical shifts (105 and 180 ppm) indicate the presence of a C=C bond in the intermediate. Therefore, two alternative structures can be proposed (Scheme 1). The chemical shifts exhibited by η^1,η^2-allyl species on ZnO[42] are in favor of but-2-en-1-ylzinc (**1**) with an internal C=C bond. On the other hand, the structure

Scheme 2. Possible Pathways of Ethene Dimerization on Zn^{2+}/ZSM-5 Zeolite: via Vinylzinc Species II (A) and via the Formation of the Bridged Intermediate IV (B)

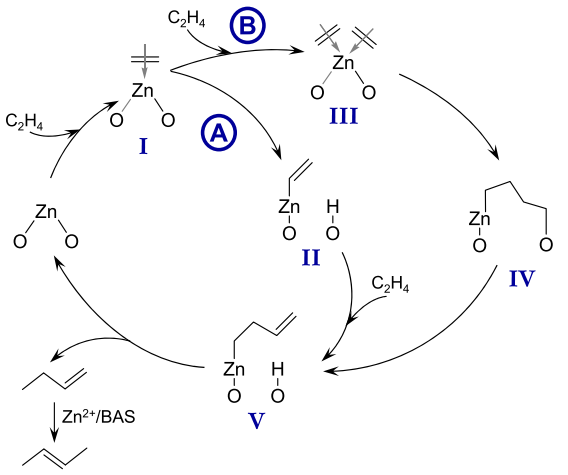

of the intermediate can be represented by but-3-en-1-ylzinc (**2**), with a terminal C=C bond, based on the chemical shifts of bis(2-methylallyl)zinc[43] with η^1,η^2-like fashion of bonding to Zn. In both cases, the C=C bonds should have π-bonding to some surface site, presumably a neighboring BAS, to explain the particular chemical shifts observed.

To further clarify the structure of the intermediate of ethene dimerization, FTIR spectroscopy was applied (Figures 2 and S5). Upon ethene adsorption on Zn^{2+}/ZSM-5 at 296 K, the characteristic bands of ethene are seen in the region of C−H bending (δ_{CH}, 1332 cm^{-1}) and stretching (ν_{CH}, 3087 and 2989 cm^{-1}) vibrations.[44] The frequency of ethene C=C stretching vibration is expectedly red-shifted to 1586 cm^{-1} (compared to 1623 cm^{-1} for gaseous ethene[44,45] and 1612 cm^{-1} for ethene adsorbed on zeolite BAS)[46] due to the formation of a π-complex with Zn^{2+} sites.[40,45] The strong interaction of ethene with Zn^{2+} sites is also indicated by the observation of the symmetry-forbidden[40,45] δ_{CH} and $\nu_{C=C}$ bands. The band at 3611 cm^{-1} corresponding to ν_{OH} of residual zeolite BAS (Si−

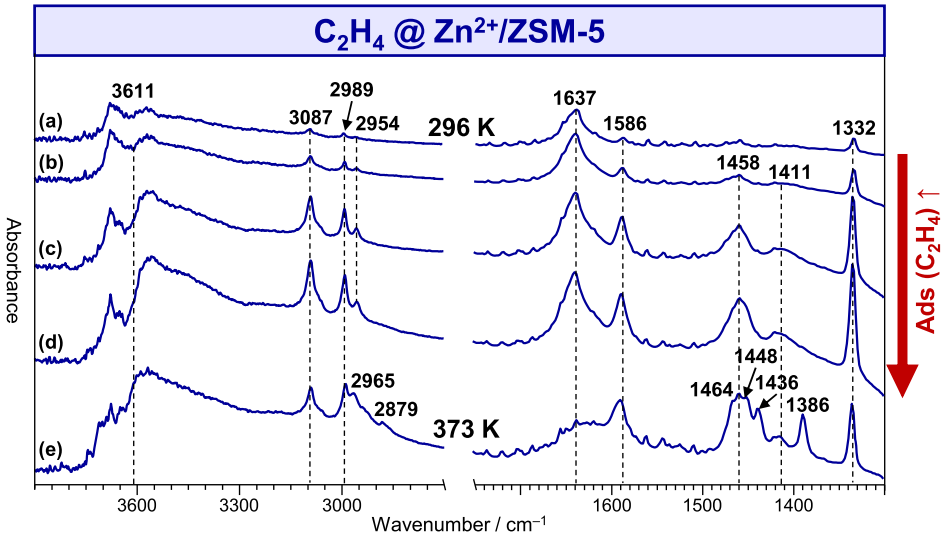

Figure 2. FTIR spectra of ethene adsorbed on Zn^{2+}/ZSM-5 zeolite, with the spectrum of pure Zn^{2+}/ZSM-5 zeolite being subtracted (see Figure S5 for the original spectra). Incremental amounts of ethene were adsorbed on the zeolite sample (a−d) at 296 K. The sample was further heated at 373 K for 5 min (e).

https://doi.org/10.1021/acs.jpcc.2c01101
J. Phys. Chem. C 2022, 126, 6570−6577

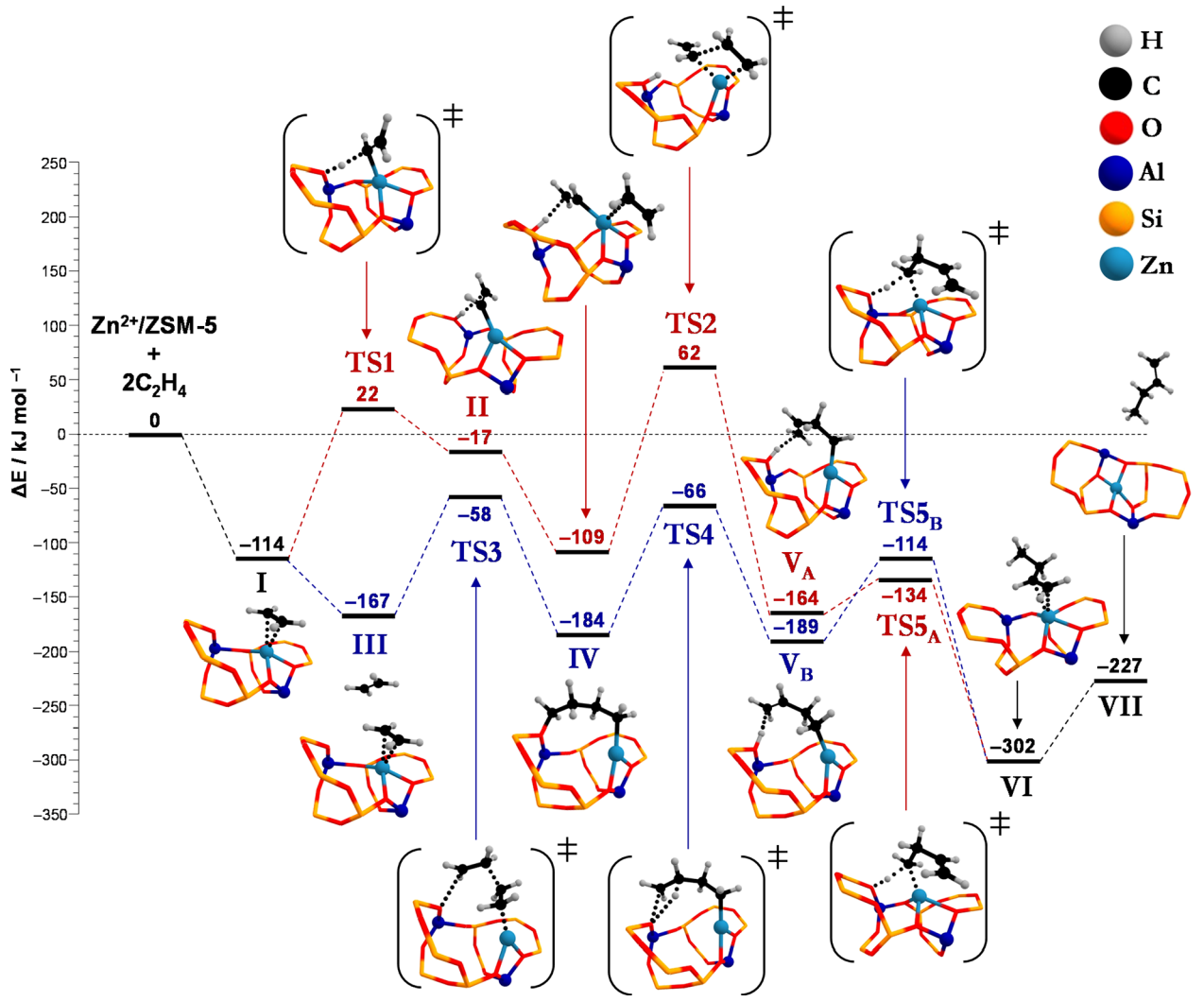

Figure 3. Calculated energy profiles and optimized structures for ethene transformation on Zn^{2+}/ZSM-5 by pathways **A** (in red) and **B** (in blue) of Scheme 2. The energies in kJ mol^{-1} have been referenced to the optimized zeolite cluster and two ethene molecules.

O(H)−Al groups) decreases, while the broad feature appears at around 3300−3500 cm^{-1} from the perturbed O−H stretching vibration due to the interaction of BAS with the adsorbed hydrocarbon species. The bands at 2954 (ν_{CH}) and 1637 ($\nu_{C=C}$) and centered at 1458 and 1411 cm^{-1} (δ_{CH}) do not belong to adsorbed ethene and can be assigned to either the intermediate or the product of ethene conversion. Heating the sample at 373 K results in the change of the spectrum, with a set of bands being almost identical to the one of 2-butene adsorbed on Zn^{2+}/ZSM-5 (Figures S6 and S7). The band at 1637 cm^{-1}, however, disappears entirely, which means that it belongs, presumably, to the intermediate detected with ^{13}C CP/MAS NMR at 296 K. The position of this band is very similar to the band of 1-butene C=C stretching,[47] and the bands at 2954, 1458, and 1411 cm^{-1} are due to the stretching and bending modes (ν_{CH}, δ_{CH}) of $-CH_2-$ and $-CH=CH_2$ fragments. Therefore, the intermediate indeed represents the C_4-fragment with the terminal C=C bond. Hence, the FTIR data are in favor of but-3-en-1-ylzinc (**2**) being the intermediate of ethene dimerization.

Thus, both MAS NMR and FTIR spectroscopy provide evidence for the selective dimerization of ethene to 2-butene on Zn^{2+}/ZSM-5 zeolite at 296−473 K. Moreover, the intermediate species, including ethene π-complex with Zn^{2+} site and but-3-en-1-ylzinc, were identified with both methods.

The formation of ethene π-complex and but-3-en-1-ylzinc implies the occurrence of ethene dimerization on a single Zn^{2+} site. Adapting the mechanisms of ethene dimerization proposed earlier for Ni- and Ga-based systems[1,10,12,48] to Zn-containing zeolite, it is reasonable to suggest two alternative pathways, **A** and **B**, of but-3-en-1-ylzinc formation (Scheme 2). But-3-en-1-ylzinc (shown as intermediate **V** in Scheme 2) is desorbed from the Zn^{2+} site as 1-butene, which is transformed to 2-butene either on the Zn sites, with the involvement of allylic intermediates, or via the olefin protonation-deprotonation on BAS.[14] The obtained spectroscopic data, however, do not allow us to distinguish between pathways **A** and **B**. While **V** is experimentally detected, neither zinc-vinyl species (**II**) nor the bridged structure (**IV**) was observed with NMR and FTIR spectroscopy. This makes it virtually impossible to experimentally determine the mechanism of **V** formation. For this reason, we have carried out a theoretical study of ethene dimerization on Zn^{2+}/ZSM-5 zeolite with the DFT method to obtain more detailed information about the reaction mechanism.

https://doi.org/10.1021/acs.jpcc.2c01101
J. Phys. Chem. C 2022, 126, 6570−6577

The calculated energy profiles for pathways **A** and **B** are presented in Figure 3. The energy of ethene adsorption and stabilization in the form of a π-complex with a Zn^{2+} site (**I**) is 114 kJ mol^{-1}. The next step, for pathway **A**, is ethene dissociation on the Zn^{2+} site to give **II** and Si−O(H)−Al group. This reaction is endothermic and has an activation energy of 136 kJ mol^{-1}. The adsorption of the second ethene molecule on the Zn^{2+} site lowers the system energy to −109 kJ mol^{-1}. The following ethene insertion into the Zn−C bond of vinylic species giving $\mathbf{V_A}$ has a rather high activation barrier of 171 kJ mol^{-1}. Following pathway **B** after **I** formation, the second ethene molecule is adsorbed, lowering the system energy by 53 kJ mol^{-1} (**III**). The formation of **IV** is exothermic and kinetically feasible, with the activation energy being equal to 109 kJ mol^{-1}. The next step of **IV** deprotonation to give $\mathbf{V_B}$ is characterized by the activation barrier of 118 kJ mol^{-1}. Note that although both pathways **A** and **B** provide the formation of but-3-en-1-ylzinc, the species $\mathbf{V_A}$ and $\mathbf{V_B}$ are not identical. They are located differently within the zeolite pore system and interact with the hydrogen atoms of structurally different Si−O(H)−Al groups (Figure S8). Both $\mathbf{V_A}$ and $\mathbf{V_B}$ can be further transformed to 1-butene π-complex (**VI**) with the Zn^{2+} site, with the activation energy being equal to 30 and 75 kJ mol^{-1}, respectively. The energy of 1-butene (**VII**) desorption from the Zn^{2+} site is 75 kJ mol^{-1}.

Therefore, theoretical investigation of ethene dimerization on Zn^{2+}/ZSM-5 zeolite shows that although both pathways **A** and **B** in Scheme 2 are possible, the pathway **B** involving **IV** is more probable, because it is characterized by lower activation barriers for all steps leading to **V** formation, than pathway **A**.

4. CONCLUSIONS

In summary, remarkably selective dimerization of ethene to 2-butene was experimentally detected on Zn^{2+}/ZSM-5 zeolite with high content of Zn^{2+} sites and low quantity of BAS at 296−473 K. The intermediate species, including π-complex of ethene with the zinc sites and but-3-en-1-ylzinc, were identified with ^{13}C MAS NMR and FTIR methods. Two alternative pathways of but-3-en-1-ylzinc intermediate formation were verified with DFT calculations. It is inferred that the pathway with the involvement of the saturated bridged dimeric Zn−$(CH_2)_4$−O species is more probable. It is shown that ethene conversion to 2-butene increases with the increase of the quantity of BAS in Zn^{2+}/ZSM-5 zeolite; however, the selectivity of the reaction decreases. The results obtained are of potential interest for developing industrially relevant Zn-containing zeolite catalysts for the selective conversion of ethene to 2-butene.

■ ASSOCIATED CONTENT

Supporting Information

The Supporting Information is available free of charge at https://pubs.acs.org/doi/10.1021/acs.jpcc.2c01101.

^1H MAS NMR spectra of benzene-$^{13}C_6$ adsorbed on Zn^{2+}/ZSM-5 and Zn^{2+}/H-ZSM-5 zeolites, cluster model of MFI-type zeolite and the local geometry of zeolite-confined Zn^{2+} cation used for DFT calculations, ^1H MAS NMR spectra of pure Zn^{2+}/ZSM-5 zeolite and ethene−$^{13}C_1$ adsorbed on Zn^{2+}/ZSM-5, ^1H and ^{13}C (CP) MAS NMR spectra of ethene−$^{13}C_1$ adsorbed on Zn^{2+}/H-ZSM-5 zeolite, FTIR spectra of pure Zn^{2+}/ZSM-5 zeolite and ethene and *n*-butene adsorbed on Zn^{2+}/ZSM-5, and optimized structures of but-3-en-1-ylzinc (PDF)

■ AUTHOR INFORMATION

Corresponding Authors

Anton A. Gabrienko − *Boreskov Institute of Catalysis, Siberian Branch of the Russian Academy of Sciences, Novosibirsk 630090, Russia;* orcid.org/0000-0002-2811-3635; Email: gabrienko@catalysis.ru

Alexander G. Stepanov − *Boreskov Institute of Catalysis, Siberian Branch of the Russian Academy of Sciences, Novosibirsk 630090, Russia;* orcid.org/0000-0003-2754-5273; Phone: +7 952 905 9559; Email: stepanov@catalysis.ru; Fax: +7 383 330 8056

Authors

Zoya N. Lashchinskaya − *Boreskov Institute of Catalysis, Siberian Branch of the Russian Academy of Sciences, Novosibirsk 630090, Russia;* orcid.org/0000-0003-1671-1301

Alexander A. Kolganov − *Boreskov Institute of Catalysis, Siberian Branch of the Russian Academy of Sciences, Novosibirsk 630090, Russia;* orcid.org/0000-0002-0262-8892

Evgeny A. Pidko − *Inorganic Systems Engineering Group, Department of Chemical Engineering, Faculty of Applied Sciences, Delft University of Technology, Delft 2629 HZ, The Netherlands;* orcid.org/0000-0001-9242-9901

Complete contact information is available at: https://pubs.acs.org/10.1021/acs.jpcc.2c01101

Funding

Russian Science Foundation, grant no. 21-73-10013. Ministry of Science and Higher Education of the Russian Federation within the governmental order for Boreskov Institute of Catalysis, project AAAA-A21-121011390053-4.

Notes

The authors declare no competing financial interest.

■ ACKNOWLEDGMENTS

The authors acknowledge the financial support from Russian Science Foundation (grant no. 21-73-10013). The maintenance of solid-state NMR and FTIR facilities used in this work was supported by the Ministry of Science and Higher Education of the Russian Federation within the governmental order for Boreskov Institute of Catalysis (project AAAA-A21-121011390053-4). We thank the Siberian Branch of the Russian Academy of Sciences (SB RAS) Supercomputer Center for providing supercomputer facilities. NWO is acknowledged for providing access to SurfSara facilities, in particular, Snellius supercomputer resources.

■ REFERENCES

(1) Al-Jarallah, A. M.; Anabtawi, J. A.; Siddiqui, M. A. B.; Aitani, A. M.; Al-Sa'doun, A. W. Ethylene Dimerization and Oligomerization to Butene-1 and Linear α-Olefins: A Review of Catalytic Systems and Processes. *Catal. Today* **1992**, *14*, 1−121.

(2) Bryliakov, K. P.; Antonov, A. A. Recent Progress of Transition Metal Based Catalysts For the Selective Dimerization of Ethylene. *J. Organomet. Chem.* **2018**, *867*, 55−61.

(3) McGuinness, D. S. Olefin Oligomerization via Metallacycles: Dimerization, Trimerization, Tetramerization, and Beyond. *Chem. Rev.* **2011**, *111*, 2321−2341.

(4) Speiser, F.; Braunstein, P.; Saussine, L. Catalytic Ethylene Dimerization and Oligomerization: Recent Developments with Nickel Complexes Containing P,N-Chelating Ligands. *Acc. Chem. Res.* **2005**, *38*, 784−793.
(5) Bonneviot, L.; Olivier, D.; Che, M. Dimerization of Olefins with Nickel-Surface Complexes in X-Type Zeolite or on Silica. *J. Mol. Catal.* **1983**, *21*, 415−430.
(6) Elev, I.; Shelimov, B. N.; Kazansky, V. B. The Role of Ni+ Ions in the Activity of NiCaY Zeolite Catalysts for Ethylene Dimerization. *J. Catal.* **1984**, *89*, 470−477.
(7) Cai, F. X.; Lepetit, C.; Kermarec, M.; Olivier, D. Dimerization of Ethylene into 1-Butene over Supported Tailor-Made Nickel Catalysts. *J. Mol. Catal.* **1987**, *43*, 93−116.
(8) Ng, F. T. T.; Creaser, D. C. Ethylene Dimerization Over Modified Nickel Exchanged Y-Zeolite. *Appl. Catal., A* **1994**, *119*, 327−339.
(9) Henry, R.; Komurcu, M.; Ganjkhanlou, Y.; Brogaard, R. Y.; Lu, L.; Jens, K.-J.; Berlier, G.; Olsbye, U. Ethene Oligomerization on Nickel Microporous and Mesoporous-Supported Catalysts: Investigation of the Active Sites. *Catal. Today* **2018**, *299*, 154−163.
(10) Joshi, R.; Zhang, G.; Miller, J. T.; Gounder, R. Evidence for the Coordination-Insertion Mechanism of Ethene Dimerization at Nickel Cations Exchanged onto Beta Molecular Sieves. *ACS Catal.* **2018**, *8*, 11407−11422.
(11) Brogaard, R. Y.; Kømurcu, M.; Dyballa, M. M.; Botan, A.; Van Speybroeck, V.; Olsbye, U.; De Wispelaere, K. Ethene Dimerization on Zeolite-Hosted Ni Ions: Reversible Mobilization of the Active Site. *ACS Catal.* **2019**, *9*, 5645−5650.
(12) Brogaard, R. Y.; Olsbye, U. Ethene Oligomerization in Ni-Containing Zeolites: Theoretical Discrimination of Reaction Mechanisms. *ACS Catal.* **2016**, *6*, 1205−1214.
(13) Gabrienko, A. A.; Lashchinskaya, Z. N.; Arzumanov, S. S.; Toktarev, A. V.; Freude, D.; Haase, J.; Stepanov, A. G. Isobutene Transformation to Aromatics on Zn-Modified Zeolite: Particular Effects of Zn^{2+} and ZnO Species on the Reaction Occurrence Revealed with Solid-State NMR and FTIR Spectroscopy. *J. Phys. Chem. C* **2021**, *125*, 15343−15353.
(14) Lashchinskaya, Z. N.; Gabrienko, A. A.; Arzumanov, S. S.; Kolganov, A. A.; Toktarev, A. V.; Freude, D.; Haase, J.; Stepanov, A. G. Which Species, Zn^{2+} Cations or ZnO Clusters, Are More Efficient for Olefin Aromatization? ^{13}C Solid-State NMR Investigation of n-But-1-ene Transformation on Zn-Modified Zeolite. *ACS Catal.* **2020**, *10*, 14224−14233.
(15) Gabrienko, A. A.; Arzumanov, S. S.; Toktarev, A. V.; Freude, D.; Haase, J.; Stepanov, A. G. Propylene Transformation on Zn-Modified Zeolite: Is There Any Difference in the Effect of Zn^{2+} Cations or ZnO Species on the Reaction Occurrence? *J. Phys. Chem. C* **2019**, *123*, 27573−27583.
(16) Chang, C. C.; Conner, W. C.; Kokes, R. J. Butene Isomerization over Zinc Oxide and Chromia. *J. Phys. Chem.* **1973**, *77*, 1957−1964.
(17) Stepanov, A. G. Basics of Solid-State NMR for Application in Zeolite Science: Material and Reaction Characterization. In *Zeolites and Zeolite-like Materials*; Sels, B. F., Kustov, L. M., Eds.; Elsevier Inc., 2016; pp 137−188.
(18) Gabrienko, A. A.; Danilova, I. G.; Arzumanov, S. S.; Pirutko, L. V.; Freude, D.; Stepanov, A. G. Direct Measurement of Zeolite Brønsted Acidity by FTIR Spectroscopy: Solid-State ^{1}H MAS NMR Approach for Reliable Determination of the Integrated Molar Absorption Coefficients. *J. Phys. Chem. C* **2018**, *122*, 25386−25395.
(19) Heemsoth, J.; Tegeler, E.; Roessner, F.; Hagen, A. Generation of Active Sites for Ethane Aromatization in ZSM-5 Zeolites by a Solid-State Reaction of Zinc Metal with Bronsted Acid Sites of the Zeolite. *Microporous Mesoporous Mater.* **2001**, *46*, 185−190.
(20) Kazansky, V.; Serykh, A. A New Charge Alternating Model of Localization of Bivalent Cations in High Silica Zeolites with Distantly Placed Aluminum Atoms in the Framework. *Microporous Mesoporous Mater.* **2004**, *70*, 151−154.
(21) Gabrienko, A. A.; Arzumanov, S. S.; Luzgin, M. V.; Stepanov, A. G.; Parmon, V. N. Methane Activation on Zn^{2+}-Exchanged ZSM-5 Zeolites. The Effect of Molecular Oxygen Addition. *J. Phys. Chem. C* **2015**, *119*, 24910−24918.
(22) Gabrienko, A. A.; Arzumanov, S. S.; Toktarev, A. V.; Danilova, I. G.; Prosvirin, I. P.; Kriventsov, V. V.; Zaikovskii, V. I.; Freude, D.; Stepanov, A. G. Different Efficiency of Zn^{2+} and ZnO Species for Methane Activation on Zn-Modified Zeolite. *ACS Catal.* **2017**, *7*, 1818−1830.
(23) Baerlocher, C.; McCusker, L. B.; Hanson, R. M. Database of Zeolite Structures. http://www.iza-structure.org/databases/ (accessed Oct 10, 2021).
(24) Arvidsson, A. A.; Zhdanov, V. P.; Carlsson, P.-A.; Grönbeck, H.; Hellman, A. Metal Dimer Sites in ZSM-5 Zeolite for Methane-to-Methanol Conversion from First-Principles Kinetic Modelling: is the [Cu-O-Cu](2+) Motif Relevant for Ni, Co, Fe, Ag, and Au? *Catal. Sci. Technol.* **2017**, *7*, 1470−1477.
(25) Mahyuddin, M. H.; Tanaka, S.; Shiota, Y.; Yoshizawa, K. Room-Temperature Activation of Methane and Direct Formations of Acetic Acid and Methanol on Zn-ZSM-5 Zeolite: A Mechanistic DFT Study. *Bull. Chem. Soc. Jpn.* **2020**, *93*, 345−354.
(26) Neese, F. Software update: the ORCA program system, version 4.0. *Wiley Interdiscip. Rev. Comput. Mol. Sci.* **2018**, *8*, No. e1327.
(27) Neese, F. The ORCA Program System. *Wiley Interdiscip. Rev.: Comput. Mol. Sci.* **2012**, *2*, 73−78.
(28) Becke, A. D. Density-Functional Thermochemistry. III. The Role of Exact Exchange. *J. Chem. Phys.* **1993**, *98*, 5648−5652.
(29) Grimme, S.; Ehrlich, S.; Goerigk, L. Effect of the Damping Function in Dispersion Corrected Density Functional Theory. *J. Comput. Chem.* **2011**, *32*, 1456−1465.
(30) Grimme, S.; Antony, J.; Ehrlich, S.; Krieg, H. A Consistent and Accurate Ab Initio Parametrization of Density Functional Dispersion Correction (DFT-D) for the 94 Elements H-Pu. *J. Chem. Phys.* **2010**, *132*, 154104.
(31) Hehre, W. J.; Ditchfield, R.; Pople, J. A. Self—Consistent Molecular Orbital Methods. XII. Further Extensions of Gaussian—Type Basis Sets for Use in Molecular Orbital Studies of Organic Molecules. *J. Chem. Phys.* **1972**, *56*, 2257−2261.
(32) Francl, M. M.; Pietro, W. J.; Hehre, W. J.; Binkley, J. S.; Gordon, M. S.; DeFrees, D. J.; Pople, J. A. Self-Consistent Molecular Orbital Methods. XXIII. A Polarization-Type Basis Set for Second-Row Elements. *J. Chem. Phys.* **1982**, *77*, 3654−3665.
(33) Rassolov, V. A.; Pople, J. A.; Ratner, M. A.; Windus, T. L. 6-31G* Basis Set for Atoms K Through Zn. *J. Chem. Phys.* **1998**, *109*, 1223−1229.
(34) Weigend, F.; Ahlrichs, R. Balanced Basis Sets of Split Valence, Triple Zeta Valence and Quadruple Zeta Valence Quality for H to Rn: Design and Assessment of Accuracy. *Phys. Chem. Chem. Phys.* **2005**, *7*, 3297−3305.
(35) Weigend, F. Accurate Coulomb-Fitting Basis Sets for H to Rn. *Phys. Chem. Chem. Phys.* **2006**, *8*, 1057−1065.
(36) Henkelman, G.; Uberuaga, B. P.; Jónsson, H. A Climbing Image Nudged Elastic Band Method for Finding Saddle Points and Minimum Energy Paths. *J. Chem. Phys.* **2000**, *113*, 9901−9904.
(37) Szécsényi, Á.; Li, G.; Gascon, J.; Pidko, E. A. Mechanistic Complexity of Methane Oxidation with H_2O_2 by Single-Site Fe/ZSM-5 Catalyst. *ACS Catal.* **2018**, *8*, 7961−7972.
(38) Szécsényi, Á.; Khramenkova, E.; Chernyshov, I. Y.; Li, G.; Gascon, J.; Pidko, E. A. Breaking Linear Scaling Relationships With Secondary Interactions in Confined Space: A Case Study of Methane Oxidation by Fe/ZSM-5 Zeolite. *ACS Catal.* **2019**, *9*, 9276−9284.
(39) Breitmaier, E.; Voelter, W. *Carbon-13 NMR Spectroscopy: High-Resolution Methods and Applications in Organic and Biochemistry*, 3rd ed; VCH: New York, 1990.
(40) Dent, A. L.; Kokes, R. J. Intermediates in Ethylene Hydrogenation over Zinc Oxide. *J. Phys. Chem.* **1970**, *74*, 3653−3662.
(41) Stepanov, A.; Arzumanov, S.; Luzgin, M.; Ernst, H.; Freude, D. In Situ Monitoring of n-Butene Conversion on H-Ferrierite by ^{1}H, ^{2}H, and ^{13}C MAS NMR: Kinetics of a Double-bond-shift Reaction, Hydrogen Exchange, and the ^{13}C-label Scrambling. *J. Catal.* **2005**, *229*, 243−251.

https://doi.org/10.1021/acs.jpcc.2c01101
J. Phys. Chem. C 2022, 126, 6570−6577

(42) Gabrienko, A. A.; Stepanov, A. G. Structure of Allylic Intermediate on Zinc Oxide, π- or σ-? *J. Phys. Chem. C* **2012**, *116*, 11096−11099.
(43) Benn, R.; Grondey, H.; Lehmkuhl, H.; Nehl, H.; Angermund, K.; Krüger, C. High-Resolution CP-MAS ^{13}C-NMR Spectra of Allylzinc Compounds − Structural Similarities and Differencies in the Solid State and Solution. *Angew. Chem., Int. Ed.* **1987**, *26*, 1279−1280.
(44) Barnes, A. J.; Howells, J. D. R. Infra-Red Cryogenic Studies. Part 12. - Alkenes in Argon Matrices. *J. Chem. Soc., Faraday Trans. 2* **1973**, *69*, 532−539.
(45) Carter, J. L.; Yates, D. J. C.; Lucchesi, P. J.; Elliott, J. J.; Kevorkian, V. The Adsorption of Ethylene on a Series of Near-Faujasite Zeolites Studied by Infrared Spectroscopy and Calorimetry. *J. Phys. Chem.* **1966**, *70*, 1126−1136.
(46) Howard, J.; Lux, P. J.; Yarwood, J. A Fourier-Transform I.R. Study of Ethene Adsorbed on HZSM-5 Zeolite at Low Temperature (295 K). *Zeolites* **1988**, *8*, 427−431.
(47) Kondo, J. N.; Liqun, S.; Wakabayashi, F.; Domen, K. IR Study of Adsorption and Reaction of 1-Butene on H-ZSM-5. *Catal. Lett.* **1997**, *47*, 129−133.
(48) Pidko, E. A.; Hensen, E. J. M.; van Santen, R. A. Anionic Oligomerization of Ethylene over Ga/ZSM-5 Zeolite: A Theoretical Study. *J. Phys. Chem. C* **2008**, *112*, 19604−19611.

https://doi.org/10.1021/acs.jpcc.2c01101
J. Phys. Chem. C 2022, 126, 6570−6577